# Unlocking the Nile Delta subsurface via advanced processing and imaging

Daniel Davies[1], Peter Brown[2], Piero Agnisola[2], Victoria Valler[2], Matvey Romanenko[2], Juergen Fruehn[2], James Raffle[2], Matthew Nicholson[3], and Sophie Pan[3]

## Abstract

The subsurface of the Nile Delta is infamous for challenges that are caused by a variety of geologic features that need to be resolved to unlock the full potential of the basin. The primary cause for many of the issues is the Messinian interval. This is a well-studied regional salt body with significant variation in composition, ranging from mobile shales to sand bodies over contaminated salt to anhydrite. The layer locally shows a hard top and base, which sets up mode conversions and complex multiples. The Messinian is also highly variable in terms of its geometry, thickness, faulting, and rugosity, which results in significant scattering of the seismic wavefield. The problem is further complicated by the presence of mud volcanoes that are scattered throughout the basin. Some of the mud volcanoes are currently active, and others are buried beneath more recent deposits. Free gas is often associated with these structures, and a high degree of lateral and vertical rock property variation is present, leading to complexities in seismic velocity and attenuation. The water depth varies considerably within the basin. Some producing assets exist that straddle the coastline, while others are located in water depths in excess of 1000 m. The transition is not simple due to erosional features on the seabed, leading to complex free-surface multiples. While many discoveries and developments have already been made in the post-Messinian, prospectivity in the basin is now located in the pre-Messinian, with targets ranging in depth from 2 to 10 km. When all of these features are combined, it results in a truly complex geophysical challenge.

## Introduction

A number of 3D towed streamer surveys were shot in the Mediterranean region between 1990 and 2005. Data sets were acquired with fairly short offsets relative to the target interval (3–5 km) and were mostly processed through prestack time migration. The broadband revolution in the early 2010s brought an update to the available seismic data (shot with longer offsets [8 km]), but significant resource progression did not transpire.

It is accepted that a complex subsurface requires further acquisition effort. Rietveld et al. (2007) highlighted uplifts obtained via multiazimuth (MAZ) seismic acquisition and processing techniques to overcome the rapidly changing Messinian and the impact it has on the pre-Messinian targets. Despite success, the technology was not widely adopted, probably due to cost. Ocean-bottom cable (OBC) surveys cover transition areas along the coastline, but they are generally acquired with sparse geometries on both the source and receiver side. While ocean-bottom recorded data gave significant uplift in other basins (Padmos et al., 2010), they used denser source effort and additionally denser receiver effort in places (Tillotson et al., 2019). In 2022, a denser shot grid ocean-bottom node (OBN) survey was acquired in the region over Atoll Field (Jiang and Lawrance, 2024). It was designed to improve pre-Messinian imaging and obtain longer offsets for full-waveform inversion (FWI).

More recently, longer-offset data have been acquired (10 km), some with simultaneous long-offset streamer acquisition in the west Mediterranean Sea with offsets in excess of 20 km. Further studies used an enhanced low-frequency source to improve the signal-to-noise ratio (S/N) for low frequencies, primarily for penetration and FWI (Tapie et al., 2023).

Thus, while acquisition solutions exist, much of the basin is covered by historical 3D data. There is some azimuthal diversity present in locations where modern acquisition overshoots existing data in different directions. However, the challenge remains to maximize the use of existing data as a cost-effective way to improve resource progression.

We present a series of case studies, all processed since 2022, that apply the latest processing techniques to historical data sets:

1) The first case study describes preprocessing techniques that improve S/N, bandwidth, and demultiple for narrow-azimuth (NAZ) streamer data.
2) The second case study resolves the impact of mud volcanoes on seismic data and the use of high-frequency dynamic-matching FWI (DMFWI) up to 20 Hz, supplemented with gravity data to overcome the challenges.
3) The third case study uses four MAZ surveys to improve velocity model building and associated image volumes.
4) The fourth case study explores the application of modern migration algorithms, FWI imaging, least-squares (LS) migration, $Q$ migration, reverse time migration (RTM), etc., along with the benefit of different products, to aid interpretation for uncertainty analysis.
5) Finally, the fifth case study highlights iterative postimage processing for improved amplitude variation with offset (AVO) attributes.

## Case study 1: Improved preprocessing

Many areas of the Nile Delta benefit from coverage of legacy NAZ towed streamer acquisition, and some have MAZ coverage.

---

[1]TGS, Houston, Texas, USA. E-mail: daniel.davies@tgs.com.
[2]TGS, London, UK. E-mail: peter.brown@tgs.com; piero.agnisola@tgs.com; victoria.valler@tgs.com; matvey.romanenko@tgs.com; juergen.fruehn@tgs.com; james.raffle@tgs.com.
[3]bp, London, UK. E-mail: matthew.nicholson@bp.com; sophie.pan@bp.com.

These surveys were commonly acquired many years apart, often without the foresight that MAZ processing/imaging would be beneficial in the future. Modern signal processing techniques can help harmonize each NAZ survey prior to final imaging. This enables the full benefit of each azimuth to be realized in the final image, maximizing the value of the extensive legacy streamer data that exist within the basin. It is commonly accepted that scattering has less of an impact on low-frequency data due to the Fresnel zone of the wavefront. Thus, careful processing of the low frequencies is vital to improve the quality of the data. No single processing step provides a one-stop solution, and careful analysis of the low frequencies at each step is fundamental to improving the preprocessed data.

Inversion-based deghosting has a significant role in improving the S/N of the low frequencies. It removes spectral notches and broadens bandwidth (Zhang et al., 2017). Often, the ghosts differ between data sets due to varying acquisition configurations. Enhancing low frequencies benefits the pre-Messinian section, which often has a peak frequency of approximately 20 Hz due to absorption and scattering through the highly complex and fractured Messinian layer. Enhancement of the low-frequency component (0–4 Hz) is critical to the success of FWI.

After deghosting is complete, the seismic record still has issues. The primary issue is multiple content, which dominates both the shallow and deep sections. The multiples can be highly complex due to a shallow water bottom, near-surface gas anomalies, proximity to mud volcanoes, and Messinian complexity. Using a combination of model-based demultiple techniques, which are carefully parameterized to target water-layer peg-leg and long-period multiples, allows accurate multiple models to be generated.

These multiple models can then be adaptively subtracted by using frequency-varying multimodel adaptive subtraction algorithms (Figure 1), which attenuates multiples while preserving primaries without risking the double subtraction of multiples.

Other key parts of the preprocessing sequence are careful matching to a master survey (when using more than one survey or if MAZ data are being used) and 4D regularization of each input survey. These are performed to a common offset scheme, giving optimal data coverage of one trace per bin per offset. A regularly sampled data set input to migration will significantly reduce migration artifacts. All input surveys are processed individually up to and including this stage, with the aim of migrating each survey individually. The reasoning behind this becomes clear during postprocessing (see the section on case study 5).

Many surveys in the area are reprocessed with the aim of planning new drilling campaigns. The presence of shallow gas makes a high-resolution image of the near surface critical for shallow-hazard assessment and analysis for future well planning and placement. We process a portion of the data at a much higher spatial and temporal resolution so the data can be used to understand drilling risks (Brookes et al., 2023). This can be achieved very effectively on legacy data by using a bespoke workflow to maximize spatial and temporal sampling, giving rise to increased bandwidth and the highest possible resolution. Once the data are deghosted, shallow-hazard-specific preprocessing branches off from the main preprocessing sequence. Demultiple and additional denoise is tailored for the shallow image by using polygons picked around shallow gas constraining such processes, allowing more targeted processing. This includes dense regularization and highly sampled migrations, which are generally
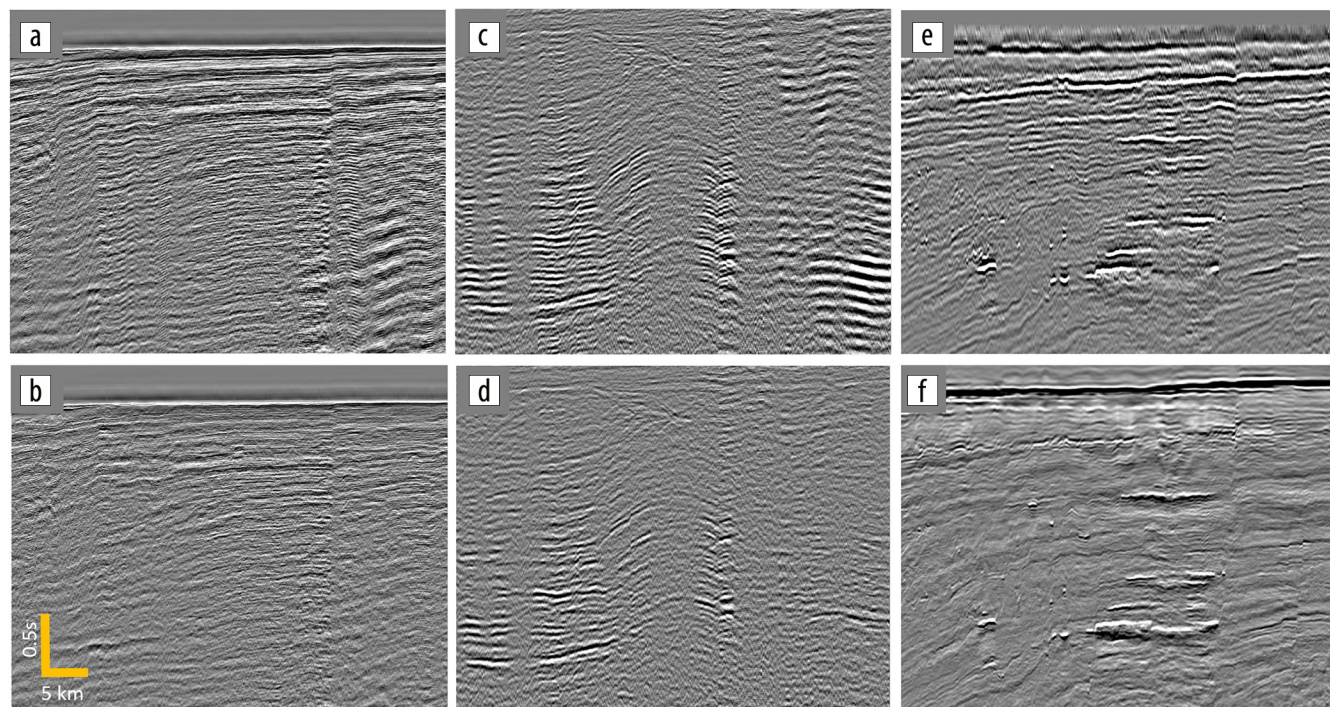


**Figure 1.** The data prior to demultiple for both (a) a shallow and (c) target interval, compared to the same sections after (b) shallow water demultiple and (d) 3D SRME. In total, five multiple models were generated and subtracted by using frequency-varying multimodel adaptive subtraction. (e) Legacy stack volume. (f) Reprocessed shallow-hazard volume. Note the clearer fault imaging and improved resolution. The image is also simplified by the application of deghosting.

not used because they are not required to image pre-Messinian structures. This proves beneficial to delineate the edges of shallow features. The data are migrated using a high-resolution velocity model that has been built with the complex shallow overburden in mind. Specific postmigration processing to enhance low- and high-frequency components of the data maximizes the value that these shallow-hazard data sets offer (see examples in Figures 1e and 1f.)

## Case study 2: Overcoming the influence of mud diapirism

While the Messinian layer poses the greatest challenge to velocity model building, there are anomalous features in the post-Messinian section, such as gas pockets and mud volcanoes, that require careful handling with FWI and tomography.

Mud volcanoes, mostly located in the post-Messinian section but with roots in the shaly layers of the pre-Messinian, are highly disruptive large edifices. Some are currently active and appear as opaque, with no clear boundaries that often protrude onto the seabed (Figure 2). Others are buried and inactive and consist of downward-tapering cones alternating with more chaotic regions (similar to the structures interpreted by Somoza et al. [2012]). For both examples, the surrounding sediment, including the Messinian section, has been deformed extensively.

During the velocity model building phase, the geometry of the mud volcanoes can be constrained through an iterative process. Initially, simple scanning for optimal starting velocities in the mud volcanoes is performed, where velocities as low as 1400 m/s can be seen in the shallowest mud volcano approximately 600 m below the seabed. Whereas, deeper in the section, they exhibit a decrease between 10% and 20% of the velocity of the surrounding rock. Because the mud volcanoes also attenuate the seismic bandwidth, we simultaneously build a model for effective $Q$. Scanning for lower $Q$ values than the background is beneficial because it reduces the dimming of events around and below the mud volcano. Typically, $Q$ values around 30 are required to sufficiently compensate phase and amplitude for further data-driven updates. Anisotropy is the third unknown inside the mud volcano. Either a low value or setting to zero is a good initial strategy.

Because the top of the mud volcano is not a coherent event, stack semblance can be used to insert the variation of $V_P$, anisotropy, and $Q$ into the model. The low semblance values define the approximate geometry of the mud volcano, which is updated in the subsequent tomography/FWI iterations by using the surrounding primary events to add detail and adjust the residual moveout/residual errors at all levels. Figure 3 illustrates this workflow by showing the impact that interpretation via stack semblance has on the Messinian structure below the mud volcano.

In the case of a buried mud volcano, velocity model building can be more straightforward because the coherent reflections inside the feeder complex (downward-tapering cones) return good data-driven updates. The base of these cones can easily be picked with a lower velocity, $Q$, and anisotropy hung from the body. If the more chaotic areas are extensive, the same stack semblance can be used as shown earlier. The low-velocity zone contributes to the tomographic update, and the perturbation image looks geologically sensible, which is an important criterion to assess the accuracy of the model. Events are clearly enhanced by the introduction of the associated update. After insertion of the mud volcano, we see an improved structural image at the edges and flanks, which simplifies the task of refining the model later in the workflow with FWI and tomography.

It is often difficult to validate this interpretative approach to velocity model building with external data points because wells are often sparse in exploration areas such as the Nile Delta. We have found that gravity data can help in this case. The observed gravity shows a pronounced low at the location of the mud volcano that is missed by the background model. Using the interpretation model discussed here, the calculated gravity trend matches the observed data more closely than the background model. This confirms that inserting a low velocity in these areas is correct.

Based on this workflow, structural detail at the relatively long spatial scale is added to the model. This allows tomography and high-frequency FWI in the post-Messinian section to converge more easily to geologically meaningful models. Figure 4 shows the results from 20 Hz DMFWI (Mao et al., 2020; Romanenko
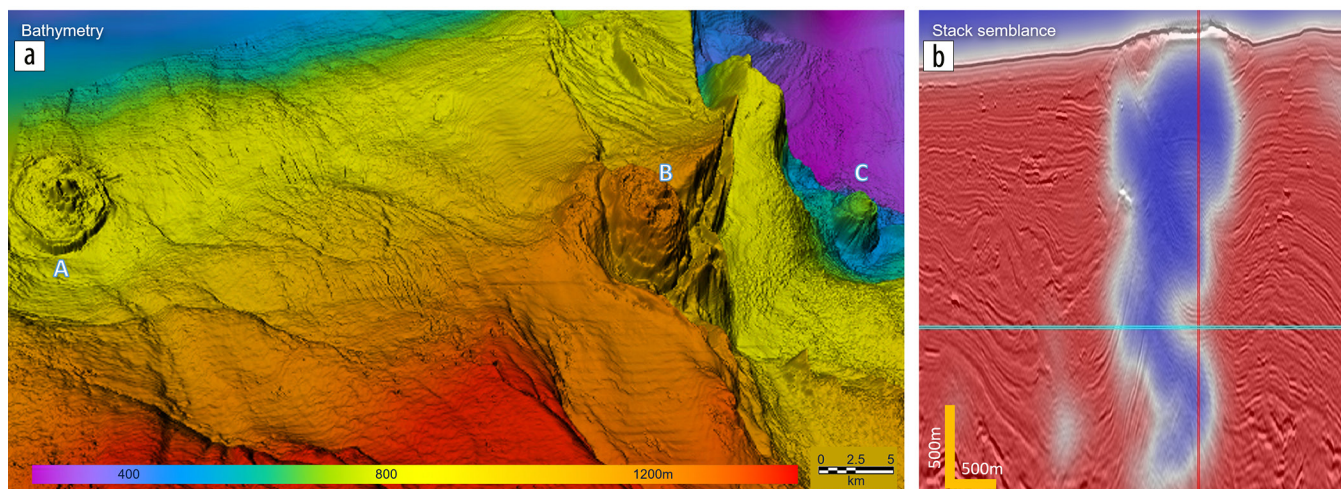


**Figure 2.** (a) Seabed morphology showing active mud volcanoes (A, B, and C). (b) Little internal structure is observed on the stack semblance. Values vary between 0 (blue) and 1 (red).

et al., 2023) for the post-Messinian section compared to the smooth starting model. FWI captures fine details such as channels, shallow gas, and the mud volcano in the center of the image.

Migration with the final model reveals a great amount of hydrocarbon-relevant detail such as realistic geometries of the mobile-shale areas and mud volcanoes, faulting, and bright spots located updip of extensional faulting. These coincide very well with a regional seeps and slicks database extracted from the 2019 Global Offshore Seepage Database (Viridien). Figure 5 shows some of these features plotted on the seabed. Figure 6 shows cross section A-A', as imaged by *Q*-RTM with the final model, together with the operators' preliminary interpretation of mud and salt in the post-Messinian section.

## Case study 3: Resolving Messinian complexity to unlock the pre-Messinian image

Although the pre-Messinian layer has a relatively simple structure, it can be highly affected by velocity inaccuracies in the complex Messinian layer. Therefore, an accurate detailed velocity model is needed to correctly image the pre-Messinian. FWI and MAZ tomography, in conjunction with some manual editing, is often used in generating velocity models. In combination with the latest high-end migration algorithms, such as *Q*-Kirchhoff, RTM, and LS *Q*-Kirchhoff, it allows us to resolve imaging issues in the target region and significantly improve the quality of final products. A smooth legacy velocity model is generally used as a starting point in the velocity model build workflow. To provide a better
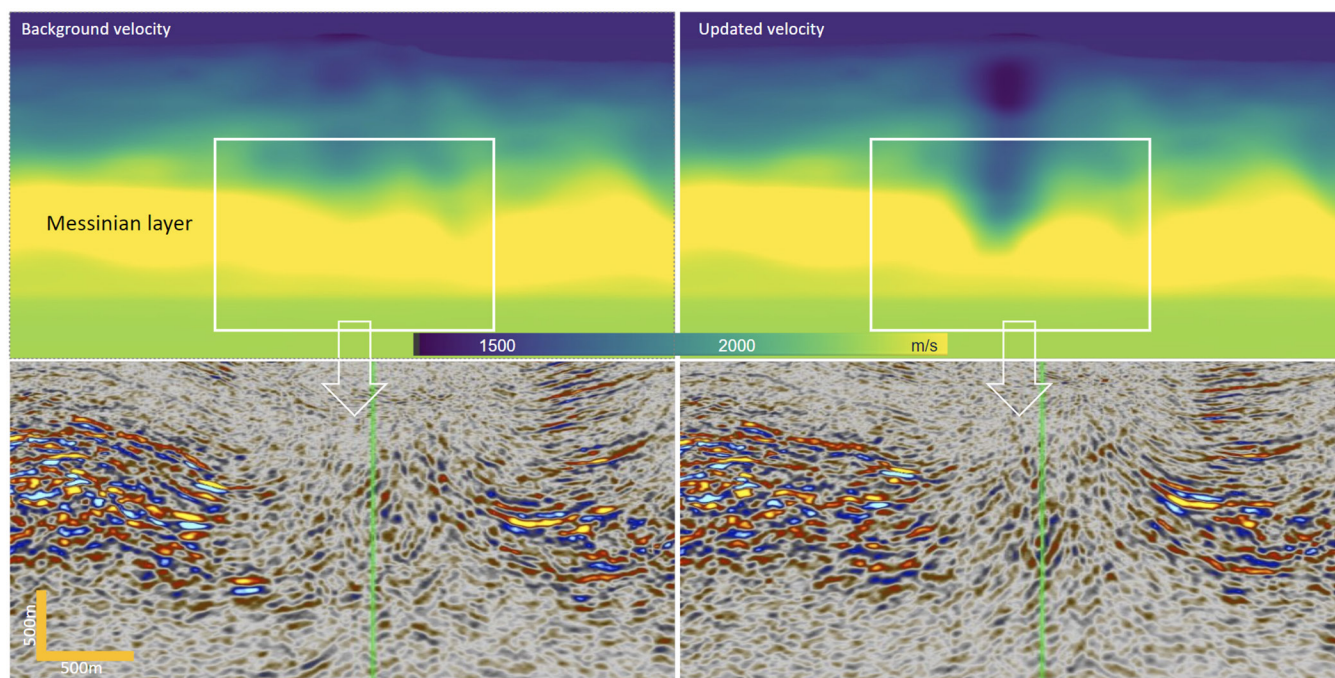


**Figure 3.** (left) Initial background model shows poor reflection continuity at the Messinian level below (bottom) the mud volcano. (right) One pass of tomography from a semblance-derived starting model significantly improves continuity at this level.
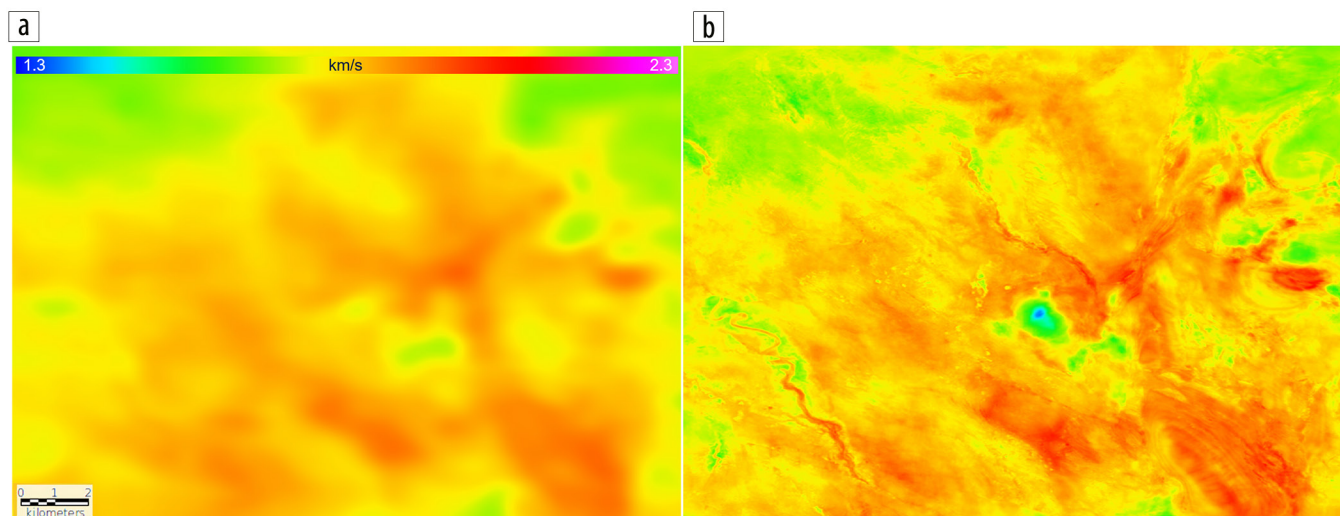


**Figure 4.** (a) Initial velocity model (smoothed legacy model) and (b) final 20 Hz FWI model at 1600 m depth. DMFWI clearly defines the mud volcano edges and channels.
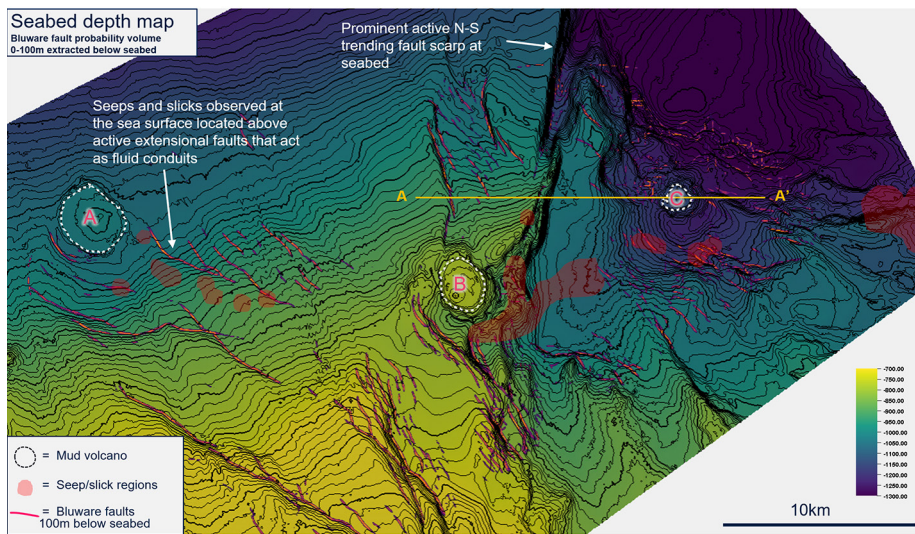
**Figure 5.** Seabed and geologic features interpreted on final RTM stack such as faults and mud volcanos (A, B, and C). A-A' is the location of the line shown in Figure 6.
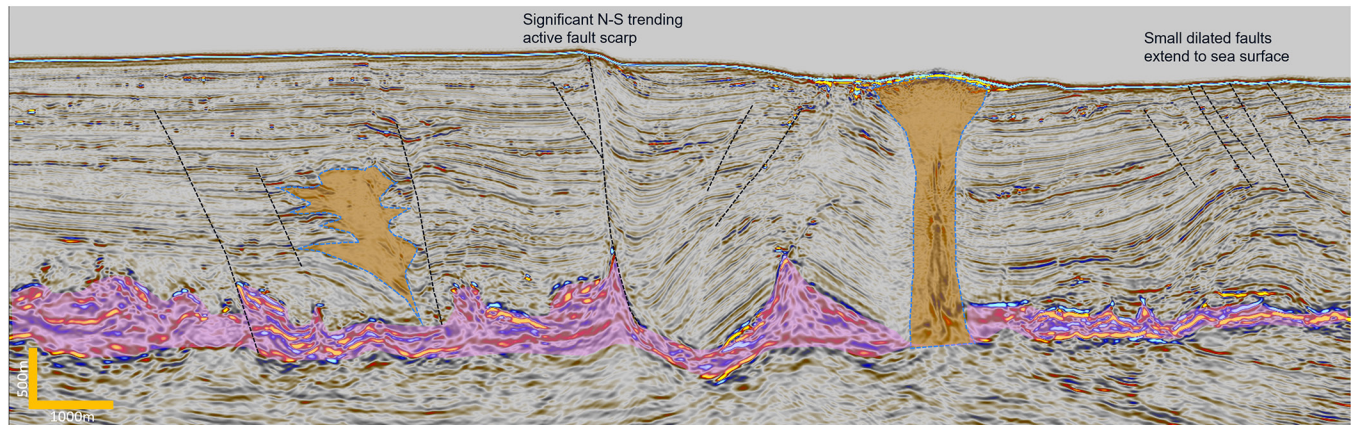
input to DMFWI and to avoid cycle-skipping, iterations of tomography may be necessary.

Streamer data typically suffer from relatively short maximum offsets (6–8 km), leading to a lack of stable refraction energy for FWI. Therefore, refraction and reflection energy are often used for a first pass of FWI to improve resolution in the post-Messinian and Messinian sections. Raw hydrophone data with minimal preprocessing can be used as an input data set. Because the data used for inversion do not have deghosting and demultiple applied, a reflective free-surface boundary generates surface multiples and ghosts in the modeled data and has a better match between observed and synthetic data.



**Figure 6.** Interpretation of mud (brown) and salt (pink) areas. Selected post-Messinian faults. A series of small dilated faults are shown extending to the sea surface (right) and a significant north–south-trending active fault scarp (center).
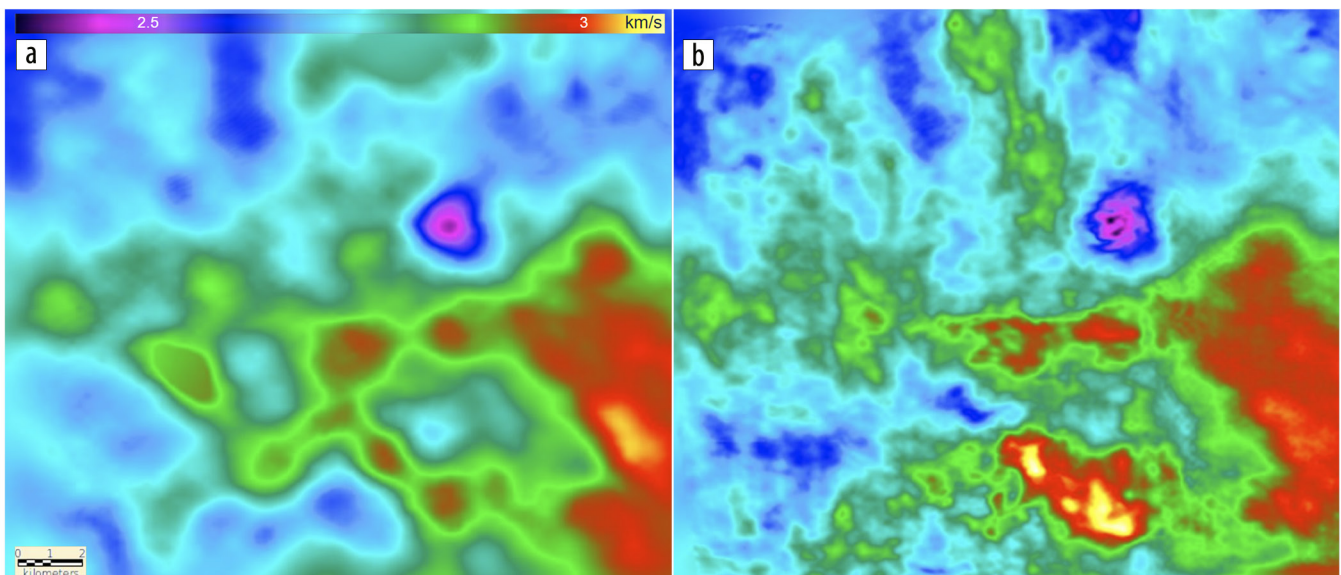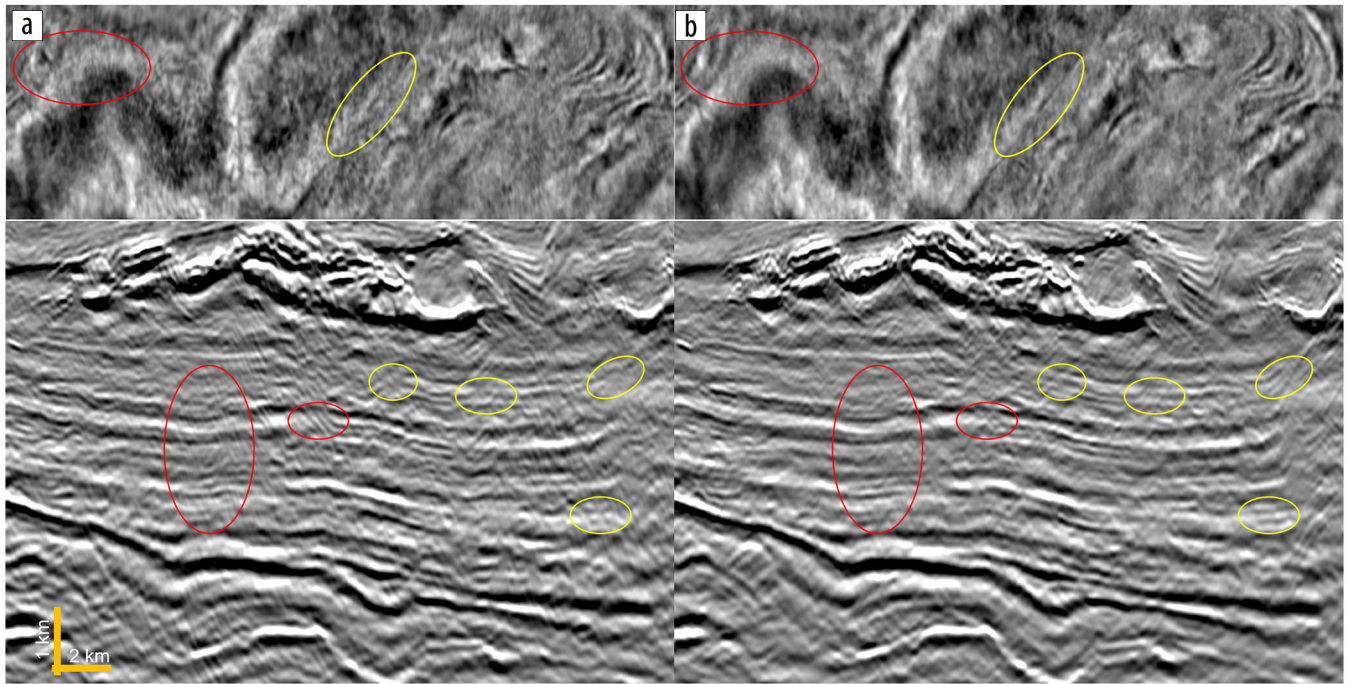


**Figure 7.** Velocity slice through the Messinian section (a) before and (b) after first-pass FWI demonstrates the uplift in resolution obtained by FWI.

**Figure 8.** Depth slice through the pre-Messinian layer and inline stack section of the FWI image using (a) one azimuth and (b) MAZ version (three azimuths). Yellow shows places with better continuity. Red shows places with less migration noise on the MAZ version.
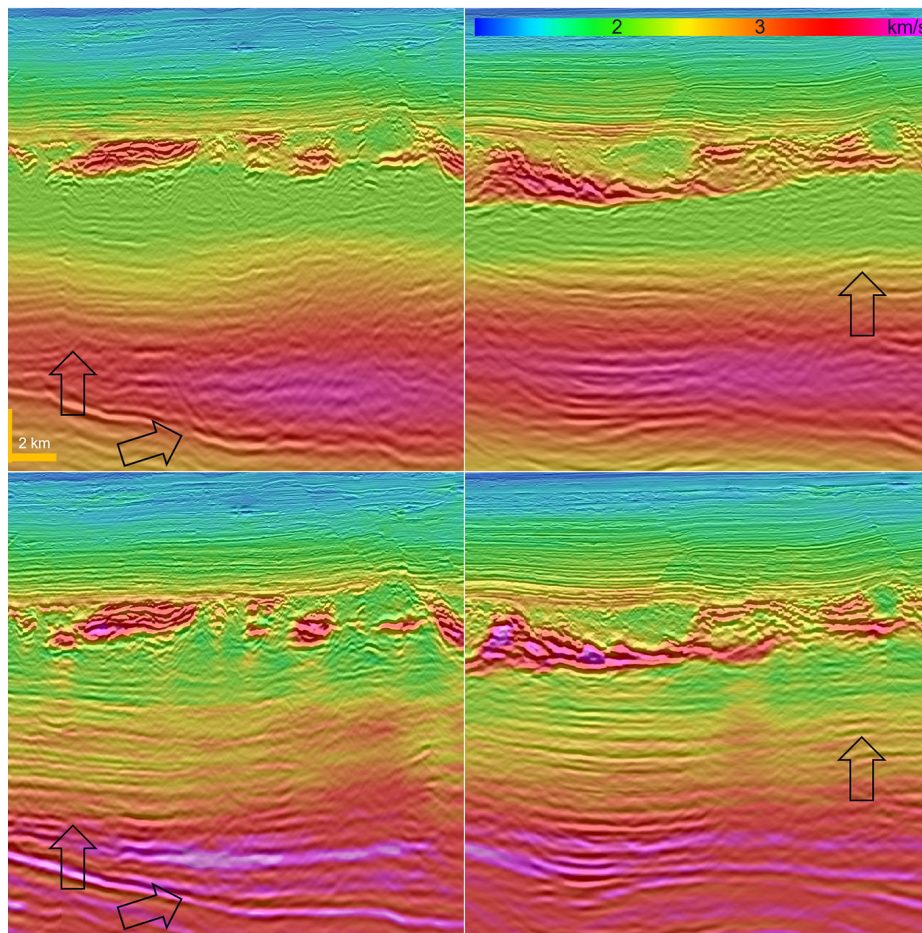


**Figure 9.** Velocity and stack (top) before and (bottom) after final pass of FWI (f3 = 20 Hz) in (left) inline and (right) crossline directions. The arrows mark locations of event deformation that are being resolved by high-resolution FWI.

In the example shown next, four frequency bands up to 10 Hz (f3 corner point; note that this is not the final frequency band) MAZ DMFWI were run, resulting in increased resolution of the post-Messinian and Messinian section (Figure 7).

The Messinian layer has rapidly varying lithologies, such as sand, shale, evaporite, and anhydrite, with no interpretable boundaries between them to allow manual interpretation. The Hilbert transform, widely used in signal processing to extract instantaneous power and phase, can help insert these lithologies as geobodies into the model. The transform, derived from a stack volume, is further processed into a mask. This allows us to reduce the low velocity associated with mobile shale and increase the velocity in the fast evaporite/anhydrite layers of the Messinian section in a data-driven fashion. With these geobodies in place, DMFWI tends to converge faster in a more geologically plausible manner.

For subsequent higher-frequency passes of FWI (to 20 Hz), it may be suboptimal to use raw hydrophone data because multiples could impact the result through crosstalk with primary events. To mitigate this, we chose to

switch to a fully preprocessed data set after demultiple, in conjunction with an absorbing free-surface boundary that generates primary events only.

The benefits of using MAZ streamer surveys for improved pre-Messinian illumination are well documented. Figure 8 shows a comparison between FWI image volumes (also called FWI-derived reflectivity) generated by single and MAZ FWI configurations. The latter has improved coherency and less migration noise. This demonstrates that building an accurate velocity model by using single-azimuth data in complex geologic areas such as the Nile Delta can be extremely challenging due to illumination issues. Therefore, MAZ acquisition is more optimal.

Variable $Q$ was introduced to compensate for the dimming of amplitudes below gas pockets and mud volcanoes. The $Q$ model was estimated from final velocities (by scaling them down to fit a $Q$ range between 30 for mud volcanoes and 110 for sedimentary layers), in conjunction with manual edits based on well information and experience in the Nile Delta area. The final model introduces small-scale detail at all levels, particularly in the Messinian layer, that resolves deformation of target events. Pullups at this level can be caused by insufficient detail in the overburden and can lead to interpretation errors, which have been significantly reduced (Figure 9).

The final high-frequency velocity model generated by DMFWI (Figure 9) not only enables accurate migrations to be produced but a detailed FWI image to be obtained. Six frequency bands of MAZ reflection DMFWI up to 20 Hz were run, resulting in clear improvement over the legacy model, with significant differences at all levels.

Because DMFWI is an LS nonlinear solution for reflection and refraction signals, FWI imaging provides more comprehensive subsurface information with better coherency, higher resolution,
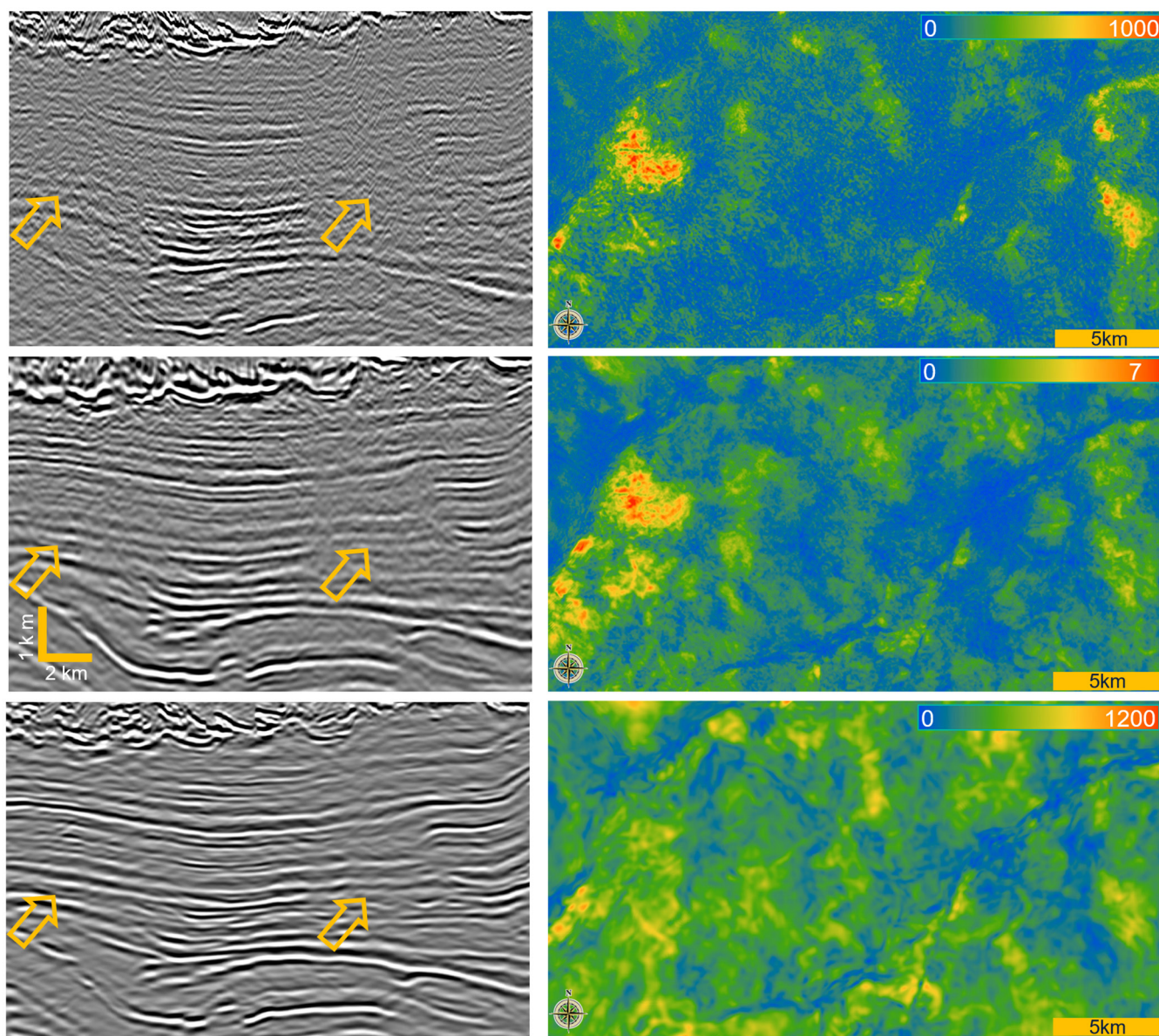


**Figure 10.** Left panel shows (top) $Q$-Kirchhoff stack, (center) $Q$-RTM stack, and (bottom) FWI image. Right panel shows RMS amplitude in the pre-Messinian. The $Q$-RTM stack is more continuous than the $Q$-Kirchhoff and shows no wave-fronting noise. The FWI image is more continuous than the RTM. The RMS amplitude also shows the increase in continuity between products.
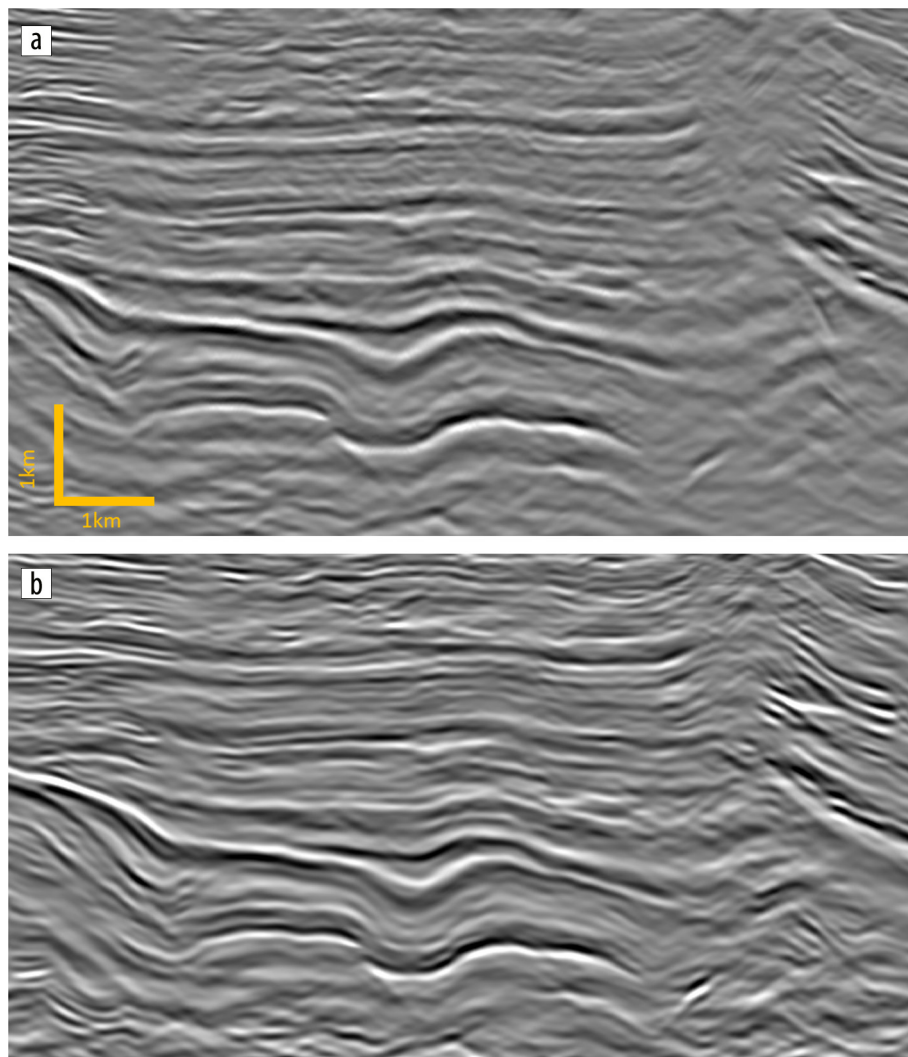
**Figure 11.** A 20 Hz FWI image (a) before and (b) after interpreter-led conditioning to enhance pre-Messinian continuity.

pre-Messinian, except in areas below shallow gas and mud volcanoes. These areas are easily identifiable by a lack of recorded amplitudes. A clear benefit of variable $Q$ migration is the reduction of dim zone and enhanced reflectivity at deeper levels. However, great care must be taken not to boost the noise at target level. Therefore, scanning for optimal gain is essential.

LS $Q$-Kirchhoff migration or LS RTM can be employed to provide further improvement of deeper reflectors and a reduction of noise in the data at the end of velocity model building. LS migrations mitigate the shortcomings in acquisition and migration approximations to improve resolution, amplitude balancing, and S/N of the migrated image. The LS process, in this case, is a single iteration process applied in the image domain, where the final production migration stacked image, which is clean and well sampled, is demigrated with the final velocity model. This creates a set of synthetic shot gathers that are migrated to form synthetic common reflection point (CRP) gathers (free of acquisition-related noise). Shaping operators are then designed in small overlapping windows, offset by offset, to make the synthetic image appear more similar to the target image. These operators are then applied to the original field data to enhance resolution and suppress noise in the field data image.

When looking at ray tracing through a complex model, such as in the Nile Delta, illumination issues at target level can easily be anticipated because the Messinian layer tends to produce irregular ray coverage of the pre-Messinian target. Therefore, ray-based algorithms, such as Kirchhoff or beam, are not optimal (top of Figure 10). In these cases, RTM can help because it can overcome the complex variability within the Messinian by handling all types of waves. As opposed to ray-based algorithms, RTM downward continues the recorded wavefield to arrive at the migrated image, ensuring better illumination of the subsurface. In addition to helping with the illumination issues, it can give better reflection continuity in the pre-Messinian. RTM does not suffer from wave fronting like ray-based algorithms and is less noisy. Figure 10 (center of Figure 10) shows a comparison between a $Q$-Kirchhoff migration and $Q$-RTM migration, where the RTM is much better illuminated and has better S/N. When comparing the FWI imaging result with the best migration result from $Q$-RTM (bottom of Figure 10), we see that FWI imaging clearly provides additional clarity and sharpness. Because FWI imaging
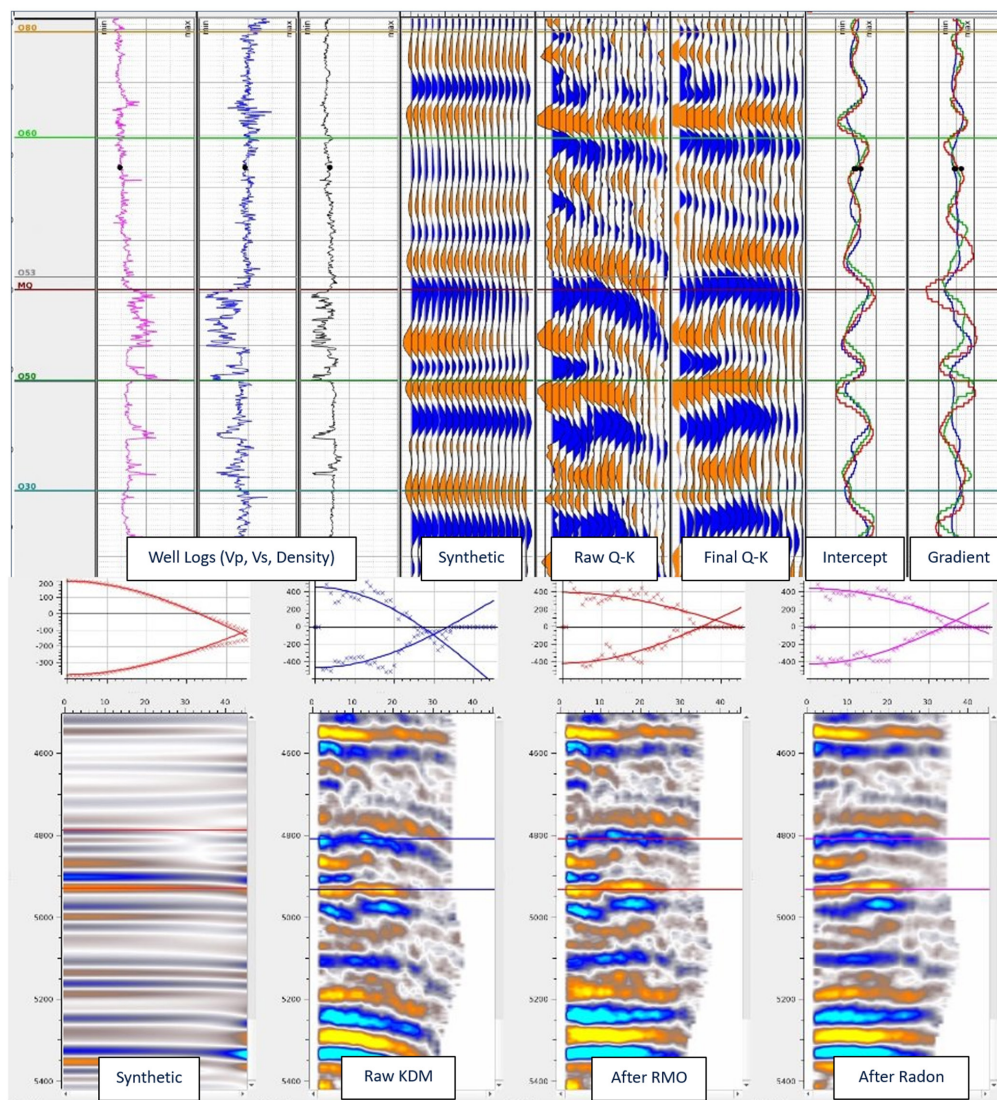
improved S/N, and better-balanced illumination in the pre-Messinian layer when compared to an equivalent Kirchhoff or RTM image. The FWI image can be used as a complementary or alternative interpretative product (see the next section on case study 4).

## Case study 4: Use of high-end migration algorithms

One of the main challenges at the pre-Messinian target level from an imaging perspective is poor S/N. Careful consideration must be given to the choice of migration algorithm. High-end algorithms such as $Q$-Kirchhoff migration, RTM, and LS migration provide a variety of benefits. In addition, FWI imaging (Wang et al., 2021) is also a form of LS imaging due to the LS inversion process involved. The FWI image is the structural derivative of the high-resolution velocity model and has been recently employed as an alternative way of imaging (Romanenko et al., 2023). In this section, we show examples of the advantages of each algorithm.

Throughout model building in the area, the velocity model improvements lead to increased continuity of reflectors in the

**Figure 12.** Example AVO QC. The top image shows available well logs and resulting synthetic. Extracted raw and final $Q$-Kirchhoff gathers at the well location and comparison of intercept and gradient. Note that the trend on the raw and final gathers closely follows the expected trend from the synthetic. The bottom image shows amplitude extractions at key horizons through postprocessing and how AVO compares to the expected trend.

is an LS solution, it has the advantages of better amplitude fidelity, reduced illumination issues, fewer migration artifacts, improved coherency, and better S/N.

## Case study 5: Iterative postprocessing for improved AVO attributes

While careful premigration processing, high-resolution model building, and the latest migration algorithms are critical for optimal conditioning and positioning of events, significant uplift can be realized by careful postmigration processing prior to the creation of an optimal MAZ image. This can reduce noise and greatly enhance interpretability below the Messinian, conditioning the data for subsequent inversion workflows.

A particularly prevalent issue can be dipping noise, partly due to the migration aperture, dip limit, and $Q$ migration. Excessive noise can degrade event continuity in low S/N areas, especially in the pre-Messinian section. Techniques such as adaptive denoise and selective attenuation in the curvelet domain improve S/N at the target while preserving fault imaging. Another benefit from

different migration algorithms, such as LS $Q$-Kirchhoff and RTM, is that the associated improvements in S/N, bandwidth, and illumination can be used to create pilot traces or models to drive denoise processes. The migrated synthetic data from each NAZ volume (created during the LS migration workflow) are used as a reference stack for iterative passes of curvelet domain denoise due to their characteristics of being relatively clean while preserving fault imaging.

Another challenge to overcome is spectral differences between the NAZ surveys. AVO-friendly spectral angle balancing can be used to further improve consistency of the spectra across all angles, compensating for frequencies attenuated at mid to far angles. Care is taken to ensure that AVO is as expected via QC against regional well trends. Further spectral enhancement can be applied poststack once noise has been attenuated.

For MAZ surveys, in order to realize the illumination benefits from individual surveys, each survey needs the flattest gathers possible that honor realistic behavior. Migrating each input

survey separately onto a common grid enables the calculation and application of separate residual moveout corrections. To correct any remaining inconsistencies between the NAZ surveys and improve the final MAZ image, trim statics can be applied in several iterative passes. Initially, trim statics are applied to individual surveys, followed by a pass to align data on each azimuth by using the MAZ stack as a pilot (similar to a 4D trim statics approach). Snail gathers before and after application of trim statics are a useful QC tool to show how traces from a common offset on each NAZ compare in terms of overall gather flatness. Once all conditioning is finalized, the individual NAZ surveys can be combined via cross-correlation-based smart stacking to give an optimal MAZ image, resolving inconsistencies in event continuity otherwise inherent in each NAZ image.

While processing contractors can use their various toolkits to condition the data, one of the most effective ways of maximizing the value of each migrated product is close collaboration with interpretation teams. This can be achieved through early delivery of volumes and iterative cycles of postprocessing. Interpretation teams benefit by receiving migrated volumes during the post-processing sequence that can be reviewed on workstations. In addition to relieving some time pressure, feedback can be used to enhance later products. An example of this can be seen in Figure 11, where an FWI image was further enhanced with additional conditioning that may not have been applied without input from the interpretation team.

Many of the targets in the Nile Delta are amplitude driven. Therefore, AVO compliance is a key metric for success. AVO QC undertaken after each stage of the postmigration workflow including intercept, gradient, and AVO crossplots, as well as comparisons to well synthetics (Figure 12), help give confidence that AVO is not impacted.

## Conclusions

We have shown through a series of case studies the value of reprocessing existing data sets in the region. A careful approach to premigration data conditioning and a data-driven but geologically grounded velocity model build contributed to a well-resolved target level. The selection of migration algorithms and final parameters to optimize the image and minimize noise and migration artifacts was also beneficial. Finally, during postmigration conditioning, an innovative and multifaceted approach to noise attenuation and the delivery of multiple products between the first Q-Kirchhoff and final LS Q-Kirchhoff rapid end-user feedback fed into the postprocessing, allowing further optimization of the final products. The use of AVO QC and comparison to well synthetics gave confidence that the products would deliver on expectations.

Close collaboration between ourselves and our clients throughout the project ensured that all objectives were met and allowed for frequent adjustments to the workflow and delivery of products to enable timely business decisions. While modern rich-azimuth long-offset low-frequency acquisition will provide significant improvements in data quality, there is much to be obtained from maximizing the use of existing and plentiful seismic data within the basin. **TLE**

Corresponding author: daniel.davies@tgs.com

## References

Brookes, D., D. Armentrout, M. Cvetkovic, T. Johnson, and T. Sullivan, 2023, High-resolution imaging in the Campos Basin using legacy seismic acquisition: Third International Meeting for Applied Geoscience & Energy, SEG/AAPG, Expanded Abstracts, 1416–1420 https://doi.org/10.1190/image2023-3911539.1.

Jiang, L., and D. Lawrance, 2024, Learning from elastic FWI and its implication for pre-Messinian imaging: First Data Processing Workshop, EAGE, Extended Abstracts, https://doi.org/10.3997/2214-4609.2024632014.

Mao, J., J. Sheng, Y. Huang, F. Hao, and F. Liu, 2020, Multi-channel dynamic matching full-waveform inversion: 90th International Annual Meeting, SEG, Expanded Abstracts, 666–670, https://doi.org/10.1190/segam2020-3427610.1.

Padmos, L., D. Davies, M. Davies, and J. McGarrity, 2010, Using high-density OBC seismic data to optimize the Andrew satellites development: First Break, **28**, no. 10, https://doi.org/10.3997/1365-2397.2010023.

Rietveld, W., J. Keggin, M. Benson, T. Manning, A. Burke, and A. A. Halim, 2007, Multi-azimuth streamer acquisition — Initial data analysis: International Petroleum Technology Conference, Extended Abstracts, https://doi.org/10.2523/IPTC-11204-MS.

Romanenko, M., L. Saxton, D. Davies, J. Sheng, F. Liu, J. Gromotka, and Y. He, 2023, High-frequency FWI on Clair OBN dataset — Challenges and successes: Third International Meeting for Applied Geoscience & Energy, SEG/AAPG, Expanded Abstracts, 1456–1460, https://doi.org/10.1190/image2023-3910442.1.

Somoza, L., T. Medialdea, R. León, G. Ercilla, J. T. Vázquez, M. Farran, J. Hernández-Molina, J. González, C. Juan, and M. Fernández-Puga, 2012, Structure of mud volcano systems and pockmarks in the region of the Ceuta Contourite Depositional System (Western Alborán Sea): Marine Geology, **332–334**, 4–26, https://doi.org/10.1016/j.margeo.2012.06.002.

Tapie, C., V. Brytik, S. Ou, L. Donaldson, A. Ouzounis, I. Fabuel-Perez, M. Guillois, et al., 2023, Optimizing seismic survey design for frontier exploration in Cyprus salt basins: Third International Meeting for Applied Geoscience & Energy, SEG/AAPG, Expanded Abstracts, 162–166, https://doi.org/10.1190/image2023-3910895.1.

Tillotson, P., D. Davies, M. Ball, and L. Smith, 2019, Clair Ridge: Learnings from processing the densest OBN survey in the UKCS: 81st Conference and Exhibition, EAGE, Extended Abstracts, https://doi.org/10.3997/2214-4609.201901182.

Wang, B., Y. He, J. Mao, F. Liu, F. Hao, Y. Huang, M. Perz, and S. Michell, 2021, Inversion-based imaging: From LSRTM to FWI imaging: First Break, Special Topic: Data Management and Processing, **39**, 85–93.

Zhang, Z., H. Masoomzadeh, and B. Wang, 2017, Evolution of deghosting process for single-sensor streamer data from 2D to 3D: Geophysical Prospecting, **66**, no. 5, 975–986, https://doi.org/10.1111/1365-2478.12614.